JOURNAL OF GEOPHYSICAL RESEARCH, VOL. 101, NO. A7, PAGES 15,737–15,747, JULY 1, 1996

Characteristics of localized ionospheric disturbances inferred from VLF measurements at two closely spaced receivers

Sean J. Lev-Tov and Umran S. Inan

STAR Laboratory, Department of Electrical Engineering, Stanford University, Stanford, California

Andy J. Smith and Mark A. Clilverd

Geospace Plasmas Group, British Antarctic Survey, Cambridge, England

Abstract. The very low frequency (VLF) NPM signal from Hawaii was recorded at two closely spaced (~50 km) receivers (located at Palmer and Faraday stations) on the Antarctic Peninsula. Measurements of characteristic amplitude and phase signatures of lightning-induced electron precipitation (LEP) events were made on three different days in March 1992. Both amplitude and, for the first time, phase measurements are quantitatively interpreted using a three-dimensional model of VLF propagation in the Earth-ionosphere waveguide in the presence of lower ionospheric disturbances. This is the first time such a study has been undertaken with mirrored precipitation. Differences between the amplitude and phase changes at the two sites are accounted for by the location of the LEP ionospheric disturbance transverse to the VLF signal propagation paths. The change in these differences is explained by the horizontal movement of the disturbance region and, therefore, the causative whistler duct footprint across the transmitter-receiver paths. Trends in the amplitude and phase changes on a timescale of order 1 hour are found to be encompassed by the modeling of the passage of the day-night terminator along the paths.

Introduction

Electron precipitation from the magnetosphere by very low frequency (VLF) waves has been observed and studied over the last several years. This includes precipitation occurring outside of the plasmasphere [e.g., *Rosenberg et al.*, 1971; *Carpenter et al.*, 1985] as well as from within the plasmasphere. This work centers on the latter: lightning-induced electron precipitation (LEP). LEP events have been observed over the last few years as characteristic amplitude and phase changes on VLF signals which propagate through the Earth-ionosphere waveguide. Typical LEP signatures have fast (<1 s) onsets, followed by a longer (10–100 s) recovery periods [*Inan and Carpenter*, 1987]. LEP signatures observed as amplitude and phase perturbations on the NPM 23.4-kHz signal from Hawaii (21.41°N, 158.15°W) to Palmer (PA) station (64.77°S, 64.05°W, $L = 2.4$) are well known and have been reported previously [*Burgess and Inan*, 1993, and references therein]; examples are in Figures 1b (amplitude) and 1d (phase). LEP events observed at PA have been linked both temporally and geographically to causative lightning (mostly in the northern hemisphere) through lightning-produced spherics and whistler waves [*Lohrey and Kaiser*, 1979; *Carpenter and LaBelle*, 1982; *Inan and Carpenter*, 1986; *Inan et al.*, 1988a, b; *Burgess and Inan*, 1990].

The gyroresonant interaction of whistler waves and geomagnetically trapped energetic electrons in the magnetosphere results in changes in the pitch angles for the electrons, which lowers the mirroring height of some of these electrons. The lowered mirror height in turn causes the electrons to precipitate into the lower ionosphere where they produce secondary ionization in the D region. These localized density enhancements constitute significant disturbances of the electrical conductivity of the nighttime lower ionosphere and alter the mode structure of the subionospheric VLF waves propagating in the Earth-ionosphere waveguide, thus leading to the observed amplitude and phase changes [*Helliwell et al.*, 1973]. The observed 10 to 100-s recovery of the signal perturbations to the preevent levels are interpreted as the transient response of the lower ionosphere which leads to the reestablishment of its chemical equilibrium state [*Pasko and Inan*, 1994].

In previous work [*Lev-Tov et al.*, 1995], direct precipitation by LEP was analyzed. In one case, causative lightning occurred on the VLF propagation path. In another case, two different crossing VLF paths were simultaneously disturbed. Only amplitude data of the LEP perturbations were available for analysis. Likely altitude electron density profiles were inferred for both the ambient ionosphere as well as the disturbance region's enhanced ionosphere.

In this paper we describe LEP amplitude and phase signatures from mirrored precipitation observed simultaneously at PA and the nearby (54 km away) Faraday (FA) station (65.25°S, 64.27°W, $L = 2.4$) on 3 nights in 1992 (March 2, 7, and 8). FA is on a bearing of 191° (as measured eastward of North) at PA so that the line joining the two stations is almost perpendicular to the NPM arrival azimuth (276° at PA); see Figures 1a and 3. In general, the natures of simultaneous signatures of an event on the two paths are nearly identical (Figures 1b-1e); however, the magnitudes of the signal changes exhibit clearly measurable differences which are interpreted here in the context of a model of VLF wave propagation in the presence of localized D region disturbances. The differences between the signal changes observed at PA and FA exhibit discernible variation over the course of the 3-hour period studied, consistent with slow (100 km/h) motion of the disturbance, and thus the associated field-aligned whistler path. The overall trends in the variation with time of the envelopes of the observed amplitude and phase perturbations are interpreted in terms of the position of the day-night terminator along the paths.

Paper number 96JA00980.
0148-0227/96/96JA-00980$09.00

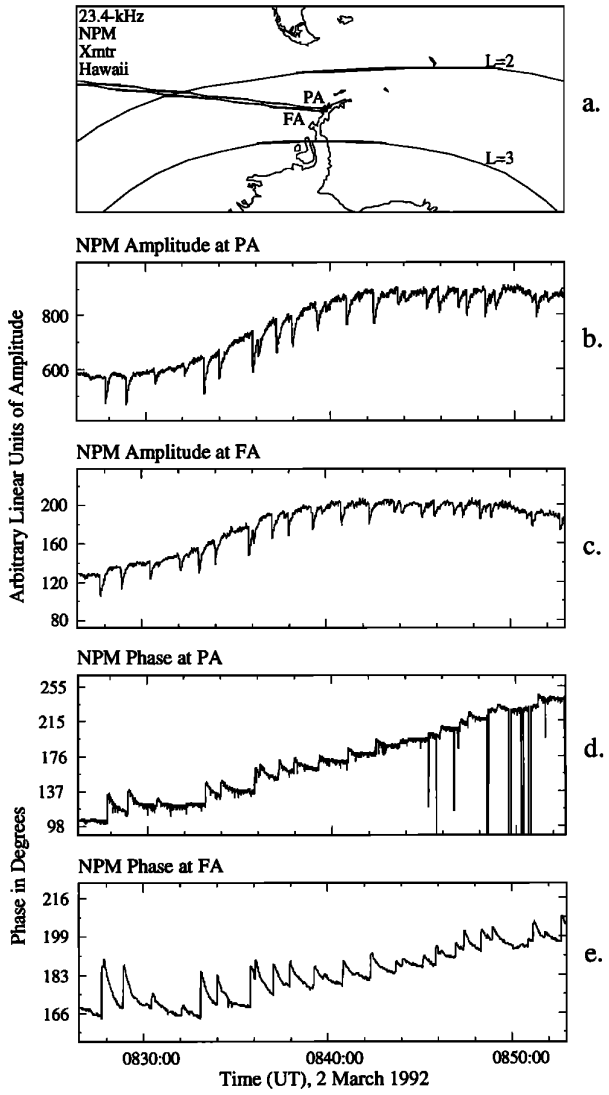

Figure 1. (a) Map showing the end of the VLF propagation paths from the NPM transmitter to the receivers at Palmer (PA) and Faraday (FA). (b) NPM signal amplitude showing LEP events recorded at PA during the March 2, 1992, episode of data. This and the three following panels share the same time axis. (c) NPM signal amplitude showing LEP events recorded at FA. (d) NPM signal phase showing LEP events recorded at PA. (e) NPM signal phase showing LEP events recorded at FA.

Experimental Data

Figures 1b-1e show a 26-min section of a 3-hour episode of LEP activity observed simultaneously at PA and FA on March 2, 1992. For the purposes of discussion in this paper, a VLF perturbation event is defined as a >0.1-dB change in signal amplitude or >1° change in phase (or both) occurring within <1 s and followed by a recovery of >10 s. Although the sizes of the VLF amplitude and phase changes vary considerably from event to event, the gross similarity of the phase and amplitude changes observed at FA and PA for each event is readily apparent. Similar episodes were also observed on March 7 and 8 and will be shown later. The temporal signatures of such events, and their association with ducted whistlers originating in lightning discharges have been extensively studied in previous work [e.g., *Inan and Carpenter*, 1986]. Every one of the characteristic signal changes shown in Figure 1 was accompanied by a ducted one-hop whistler (from a lightning flash in the northern hemisphere) observed at PA station. The whistler rate was ~3.4 whistlers per minute during the observation period, and showed no signs of decrease toward the end of the period. In this paper we concentrate on quantitative interpretation of the VLF signal amplitude and phase changes and their variations over time.

Figures 2a and 2b show the measured amplitude and phase changes, respectively, for each of the events observed during 0650–1000 UT on March 2, 1992. As noted, generally similar signal changes were observed at FA and PA. Amplitude and phase changes ranged from −2.0 to +0.4 dB and 0 to +27°, respectively. During the early period when the best defined events were observed, the amplitude changes were negative and the phase changes were positive, as expected on this ~12 Mm (1 Mm = 10^6 m) long and entirely sea-based VLF path [*Inan and Carpenter*, 1987]. Starting at ~0830 UT, the amplitude changes gradually became positive, and the phase changes showed a marked decrease in magnitude. This same trend was also observed on March 7 and 8, 1992 (Figure 9) and is interpreted in terms of the position of the day-night terminator along the propagation paths, as discussed in a later section.

Figures 2c and 2d show the differences between the amplitude and phase changes observed at FA and PA. Although small in magnitude compared to the changes themselves, these differences of up to 0.6 dB in amplitude and 9° in phase are generally well above the estimated measurement uncertainty (±0.05 dB and ±0.5°). Careful examination of Figure 2c also shows that the quantity $\Delta A_{dif} \equiv \Delta A_{FA} - \Delta A_{PA}$ exhibited a general trend during the course of the period, changing from largely negative values until ~0830 UT to largely positive values in the later periods. The range of values of ΔA_{dif} and its variation with time are interpreted by means of the model described below.

Model Formulation and Results

A computer-based model of subionospheric VLF propagation and scattering in the presence of localized disturbances [*Poulsen et al.*, 1993a] was employed to interpret the VLF signal changes observed in this case study. The model is based on a multi-mode representation of the VLF signal propagating in all three dimensions through the Earth-ionosphere waveguide. The ambient ionospheric electron density and temperature profiles can be arbitrarily specified anywhere along the propagation path, as well as the realistic values of ground conductivity and of the Earth's magnetic field. The characteristics of the ionospheric disturbance, such as horizontal extent, location, and enhanced ionospheric electron density profile are also external inputs to the model. The signal changes observed at any receiving locations are determined as the difference between the signal amplitude/phase under ambient conditions versus their values in the presence of the disturbance.

Disturbance Location, Ambient and Disturbed Ionization Profiles, and Other Factors

In terms of the model calculations, it is important to note that the resultant amplitude and phase changes are not strongly dependent on the location of the disturbance along the long sea-based NPM path, provided it is not within a few hundred kilometers of the receiver [*Poulsen et al.*, 1990; *Lev-Tov et al.*, 1995], so that the particular choice of the disturbance location along the path is not critical to the main purposes of the paper. However, the amplitude and phase changes do depend sensitively on the disturbance location

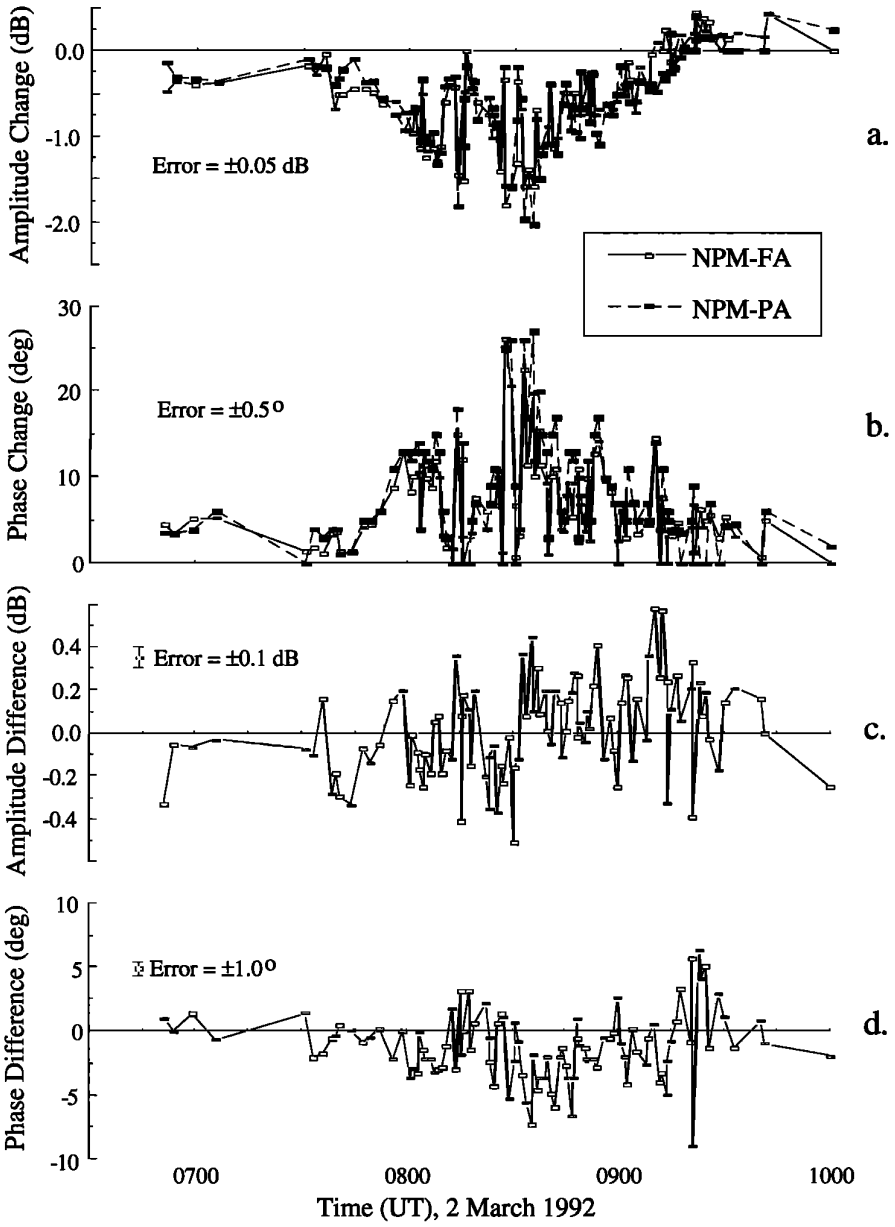

Figure 2. (a) Amplitude changes of the NPM signal received at both PA and FA during the episode of March 2, 1992. The measurement error is ±0.05 dB. All four panels in this figure share the same time axis. (b) Phase changes of the NPM signal received at both PA and FA. The measurement error is ±0.5°. (c) The difference between each amplitude change recorded at FA and the simultaneous amplitude change recorded at PA ($\Delta A_{dif} \equiv \Delta A_{FA} - \Delta A_{PA}$). The resulting error is ±0.1 dB. (d) The difference between each phase change recorded at FA and the simultaneous phase change recorded at PA ($\Delta\Phi_{dif} \equiv \Delta\Phi_{FA} - \Delta\Phi_{PA}$). The resulting error is ±1.0°.

transverse to the path [*Poulsen et al.*, 1990]. The fact that the PA-FA baseline is nearly perpendicular to the NPM-PA and NPM-FA lines suggests that the differences between observations at PA and FA might be due to the transverse distance between the disturbance and the paths. A 400-km scan line perpendicular to the NPM-PA and NPM-FA paths, centered midway between them, and 2.0 Mm from PA and FA was chosen as the locus of points along which to vary the location of the disturbance (Figure 3). Time-correlated whistlers observed with a broadband direction-finding receiver at PA were determined (via whistler analysis) to have propagated on magnetospheric ducts located at $L \simeq 2.1$ and due north of PA. These whistlers, however, are unlikely to have caused the LEP signatures observed on the NPM path, since the ionospheric footprints of their ducts (and thus the disturbance locations) would be too far from the path [*Poulsen et al.*, 1990; *Lev-Tov et al.*, 1995]. Previous work [*Burgess and Inan*, 1993] suggests that ducted whistlers observed at PA and associated with LEP events on the NPM-PA signal originate from ionospheric exit points lying in close proximity to the path. We therefore assume that the causative whistlers in the March 2, 1992, case, although excited by the same northern hemisphere source as

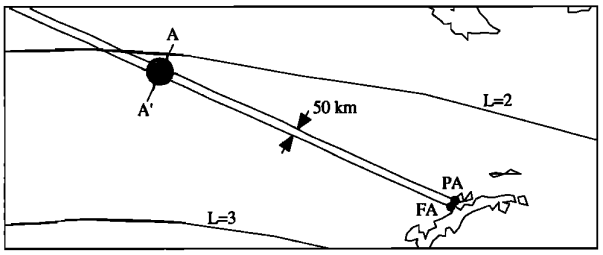

Figure 3. Map showing location of scan line (AA′) for ionospheric disturbance positions used in modeling. The scan line is 400 km long and centered about the midpoint between the two paths. The disturbance shown (shaded circle) is at the center of the scan line and it is 150 km in diameter.

the whistlers received from the northerly direction, traveled in one or more ducts at approximately the same L shell (i.e., $L \simeq 2.1$), but were located along the NPM-PA path, putting them at a distance of ~2 Mm from PA and thus below the detection threshold at PA. This circumstance is consistent with the fact that LEP events were observed until the day-night terminator reached a position of ~2 Mm from PA and FA (which is about where $L = 2.1$ and the two paths intersect; see Figure 3), as discussed in later sections.

Nine different ambient and disturbed ionospheric electron density profile combinations were considered in the model. The three ambient profiles (1, 2, 3) are displayed in Figure 4a. They span a 1:10:100 range in electron density values around the middle of the 70 to 90-km range, near the nighttime VLF reflection height. Profile 1 is a tenuous nighttime ionosphere represented by an exponential curve [*Wait and Spies*, 1964; *Wait*, 1966]. Profile 2 is a typical nighttime ionosphere [*Reagan et al.*, 1981]. A dense nighttime ionosphere is exemplified by profile 3 [*Inan et al.*, 1992]. The top portion of each of these profiles (above 97 km for profile 1, above 90 km for profile 2, and above 95 km for profile 3) is taken from the International Reference Ionosphere [*Rawer et al.*, 1978].

The three electron density profiles representing the secondary ionization enhancement produced in the D region by the LEP bursts are shown in Figure 4b. Each enhancement profile can be added to an ambient profile of Figure 4a to obtain the total perturbed electron density profile at the center of the LEP disturbance (assumed circular). For example, Figure 4c has the total enhanced electron density profiles corresponding to the enhancements of Figure 4b when added to ambient profile 2 (Figure 4a). The enhancements of Figure 4b are expected for a 0.2-s LEP burst duration and a peak flux of 5×10^{-3} ergs cm^{-2} s^{-1} when ducted magnetospheric whistlers range in frequency from 0.5 to 6 kHz and the whistler-particle interactions occur near the geomagnetic equator at L shells of 1.5–2.5 [*Chang and Inan*, 1985]. For a more detailed description of the enhancement profiles, the reader is referred to *Lev-Tov et al.* [1995].

In all cases, the exponential altitude profile of collision frequency given by *Wait and Spies* [1964, 1965] was used for the electron-neutral particle (ν_e) collision frequency. It is

$$\nu_e(z) = 1.816 \times 10^{11} e^{-0.15z}$$

where ν_e is in hertz and z is the altitude in kilometers.

We assume the electron density enhancement (ΔN_e) to have a Gaussian dependence in the radial direction, so that at any given altitude, the density enhancement is given by

$$\Delta N_e(r) = \Delta N_e(r = 0) e^{-(r/r_0)^2}$$

Based on past experimental evidence indicating that the diameter of LEP disturbances is likely to be 100–300 km [*Inan et al.*, 1988b, 1990; *Lev-Tov et al.*, 1995], disturbance radial scales r_0 in the range of 75–150 km were used in our model calculations.

Several different factors affect the magnitude, transverse size, and altitude profile of the ionospheric disturbances arising from LEP bursts and hence the resultant amplitude and phase changes observed on VLF signals [*Burgess and Inan*, 1993; *Lev-Tov et al.*, 1995]. An important factor is the fact that the intensity of the lightning discharge, the radiated fields, and the resultant intensity of the magnetospheric whistler vary from event to event. Variations in the precipitated flux levels occur both due to different whistler intensities and due to changes in the trapped flux levels [*Inan et al.*, 1989]. The cross section of the whistler-mode propagation duct

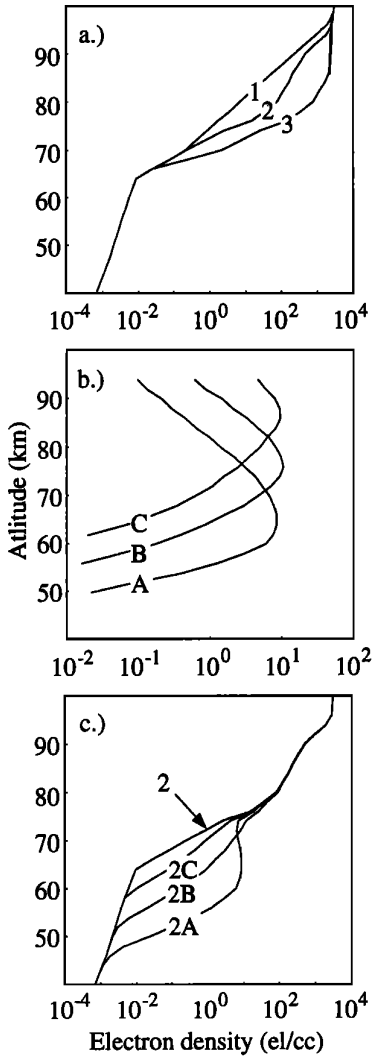

Figure 4. Nighttime electron density profiles used in this work. (a) Three ambient nighttime electron density profiles varying from a tenuous (1) to a dense (3) D region in a 1:10:100 range in the middle of the 70 to 90-km portion of the ionosphere where VLF reflection occurs at night. (b) The excess ionization which is added to the ambient electron density profiles (Figure 4a) to obtain the profile at the center of the LEP disturbance (e.g., Figure 4c). (c) The electron density profiles which were assumed to be in effect at the center of the disturbed regions. For the case illustrated, the ambient profile 2 is shown with the three ionization enhancements of Figure 4b.

(likely to remain constant during an event episode) determines the transverse extent of the disturbance. The altitude profile of the electron density enhancements is determined by the energy spectrum of the precipitating electrons, which itself is a function of several factors: the whistler frequency spectrum, the plasma frequency, the electron gyrofrequency (i.e., L shell), and the energy spectrum of the trapped electron distribution at pitch angles near the loss cone [*Inan et al.*, 1989]. For a given disturbance with specified size and altitude profile of density enhancement, the magnitude of the VLF signal changes depends sensitively on the disturbance distance from the great circle path [*Poulsen et al.*, 1990]. An additional important factor is the ambient nighttime ionospheric electron density altitude profile which sets the VLF reflection height, thereby affecting the mode structure of the VLF signal when it encounters the disturbance [*Lev-Tov et al.*, 1995]. The modeling effort presented in this paper explores the roles of the ambient and disturbed electron density profiles, the position of the disturbance transverse to the great circle path, the horizontal extent of the disturbance, and the effect of the day-night terminator. While it is clear that event-to-event variations due to the other factors occur, the overall trends in the envelope of the measured quantities can be interpreted in terms of these mostly ionospheric factors.

Results

We first consider the dependence of the signal amplitude and phase at the receiver (PA or FA, but taken to be PA here) on the ambient ionospheric electron density profile. Figure 5 shows the signal amplitude variation along the NPM-PA path as well as the waveguide mode structure of the modes dominant at the receiver (PA). The waveguide modes are identified as being quasi-transverse magnetic (QTMn) or quasi-transverse electric (QTEn) where n is the order of the mode [*Poulsen et al.*, 1993a]. For the cases of profiles 1 and 2, the QTM2 mode is dominant at PA, having ~10 dB larger intensity as compared to the next highest mode (QTE1 for profile 1 and QTM1 for profile 2). That this would be the case for the NPM-PA path under conditions of an exponential density profile (profile 1) was noted before [*Inan and Carpenter*, 1987; *Poulsen et al.*, 1990]. However, we note that for profile 3 the two modes QTM1 and QTM2 have comparable (within 10% of each other) amplitudes. As these two modes interfere with one another, deep nulls occur at spaced locations along the propagation path, with one of the nulls being very close to PA. In general, the presence of a null near the receiver significantly increases the sensitivity of the received signal to ionospheric disturbances [*Tolstoy*, 1983; *Barr et al.*, 1985; *Tolstoy et al.*, 1986; *Poulsen et al.*, 1993a], so that lower ionospheric disturbances of given characteristics would lead to larger ΔA and $\Delta\Phi$ under conditions of profile 3 than they would for the cases of either ambient profile 1 or 2.

The amplitude and phase changes predicted by the model for the NPM-PA path and for a 150 km diameter disturbance (r_o = 75 km) are shown in Figure 6 for all nine profile combinations (the three ambient profiles 1, 2, and 3, and the three enhanced profiles A, B, and C, all from Figure 4). Each curve is presented as a function of disturbance position along the scan line (AA′ in Figure 3). Similar results were obtained for the NPM-FA path. As expected, the largest values of ΔA and $\Delta\Phi$ occur for ambient profile 3. In fact, for the peak precipitation flux level assumed in establishing the profiles (5×10^{-3} ergs cm^{-2} s^{-1}), LEP bursts occurring under conditions of profiles

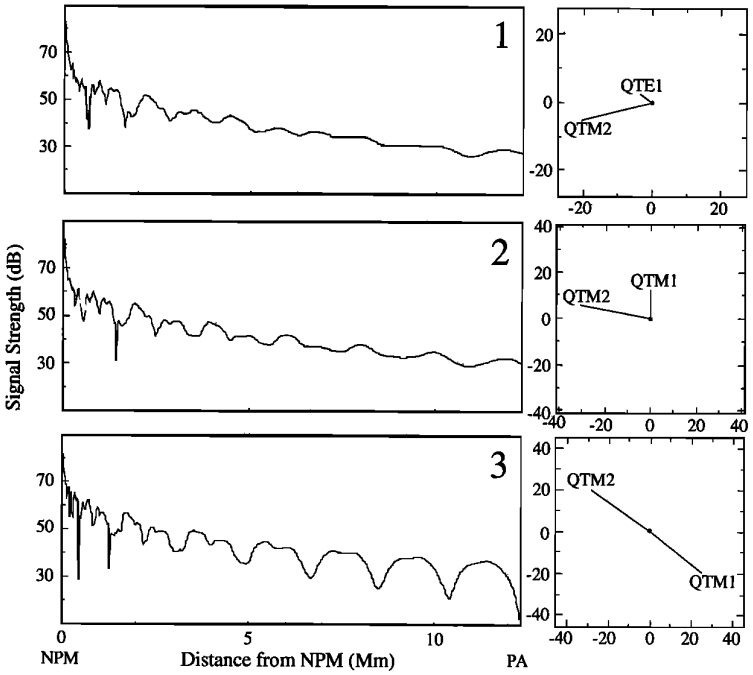

Figure 5. NPM signal amplitude along the NPM-PA path (total length = 12.35 Mm) for the three different ambient ionospheric electron density profiles (Figure 4a). To the right of each of these figures is the mode structure showing the relative amplitudes and phases of the vertical electric fields of the dominant modes at the receiver (PA) during quiet (no disturbance) conditions. QTMn (quasi-transverse magnetic) and QTEn (quasi-transverse electric) modes are numbered by order n. The mode vectors are shown in arbitrary units since we are concerned quantitatively only with changes in the signal (from LEP) and not actual signal levels. We note the deep nulls, especially the one at PA, when profile 3 is in effect due to the signal's having two dominant modes (within 10% of each other).

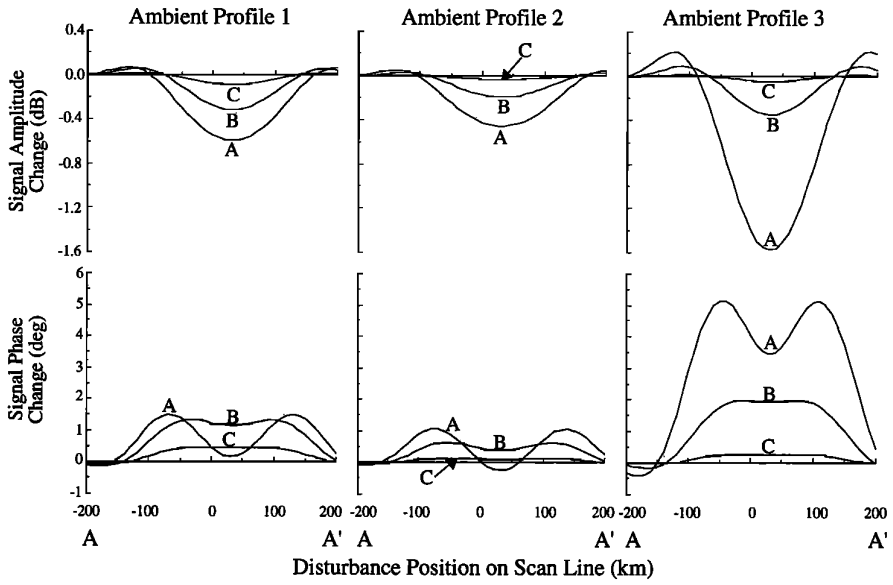

Figure 6. Each curve in the top row shows the predicted VLF signal amplitude change on the NPM signal at PA as a function of the location of a 150-km-diameter disturbance on the scan line AA′ (Figure 3). The bottom row displays corresponding signal phase changes. Each column of the figure corresponds to one of the three ambient nighttime electron density profiles (Figure 4a). Curves are labeled to correspond to the electron density enhancements of Figure 4b.

1 and 2 lead to ΔA and $\Delta\Phi$ values far smaller than those observed. Note that substantially larger precipitation fluxes would be highly atypical; in the only existing set of in situ satellite observations of LEP bursts on the SEEP satellite, the largest fluxes observed were 10^{-2} ergs cm^{-2} s^{-1} [*Voss et al.*, 1985]. Of the three different disturbances, and for the ambient profile 3, enhancement profile A leads to the largest perturbations. Note that this profile represents ionization enhancements at the lowest altitudes, thus corresponding to the highest energy content of the precipitation electrons.

Figure 7 shows model results for NPM-FA and NPM-PA, for ionospheric profile combination 3A; the variations of the amplitude and phase changes with distance from the path are very similar for the almost coincident paths except for the lateral shift corresponding to separation. For the amplitude data, both the sign and size of the changes themselves (Figure 2a, ΔA_{PA} and ΔA_{FA}) and also the differences between NPM-PA and NPM-FA (Figure 2c, ΔA_{dif}), are consistent with the model predictions (top panel of Figure 7) as we discuss further in the next section. Some of the observed phase changes, however (Figure 2b, $\Delta\Phi_{PA}$ and $\Delta\Phi_{FA}$), ranging up to 27°, are not in good agreement with the lower panel of Figure 7 but are consistent with a larger disturbance diameter $d = 2r_o$ (up to 300 km): Table 1 shows amplitude and phase changes for disturbances of different characteristics located on the NPM-PA path at a distance 2.0 Mm from PA. Note that the expected values for a 300-km-diameter disturbance with profile combination 3A are −3.3 dB and 20°, respectively. Figure 8 shows that larger differences between the two sites (ΔA_{dif} and $\Delta\Phi_{dif}$) can be explained by a larger disturbance (using profile combination 3A): amplitude differences are up to 1.6 dB and phase differences are up to 7°.

Discussion

Our model results presented above were based on the inference that the disturbance was located at $L \simeq 2.1$, nearly along the NPM-PA (or NPM-FA) baseline at a distance ~2 Mm from the stations, and are not sensitive to the disturbance location along the path [*Poulsen et al.*, 1990; *Lev-Tov et al.*, 1995]. Within the context of this assumption, the comparison of model results with data indicates that a disturbance located within ±200 km of the paths and having a size ≤300 km can account for the observed range of the amplitude and phase changes. For a reasonable precipitation flux level of 5×10^{-3} ergs cm^{-2} s^{-1}, the profile combination 3A provides the best fit to the data. However, some other profile combinations with higher precipitation fluxes or larger disturbance regions would also be consistent with observations, as discussed below. Ambient profile 3 (Figure 4a) represents a dense nighttime ionosphere which leads to a deep null in signal intensity near the receivers (Figure 5), providing for very high sensitivity to ionospheric disturbances. Enhancement profile A is the most deeply penetrating disturbance (Figure 4b), which would be produced by precipitating electrons with energies >600 keV; at $L \simeq 2.1$, whistler frequencies <1.2 kHz would cause the precipitation of such electrons [*Chang and Inan*, 1983]. Disturbance profile A was determined likely to have been in effect in our previous work [*Lev-Tov et al.*, 1995]. Variability in the size of the amplitude and phase changes from event to event can be understood in terms of the variability in other factors influencing the LEP process, such as the lightning-whistler frequency spectrum and intensity, and trapped flux intensities and spectra. It is not likely that disturbance position and size changed from event to event since these are determined by the characteristics of the whistler-mode duct, which would be expected to remain constant on a timescale of minutes [*Carpenter*, 1966].

The findings reported above also support the magnitudes of the differences in amplitude changes between the measured values at FA and at PA (Figures 2c and 2d). These differences are likely to be due to the differing transverse positions of the disturbance relative to each of the paths (Figures 7 and 8). Figure 2c shows that the amplitude difference (ΔA_{dif}) between FA and PA during an hour centered around 0830 UT changed from being mostly negative to mostly positive. The envelope of the phase differences ($\Delta\Phi_{dif}$) also

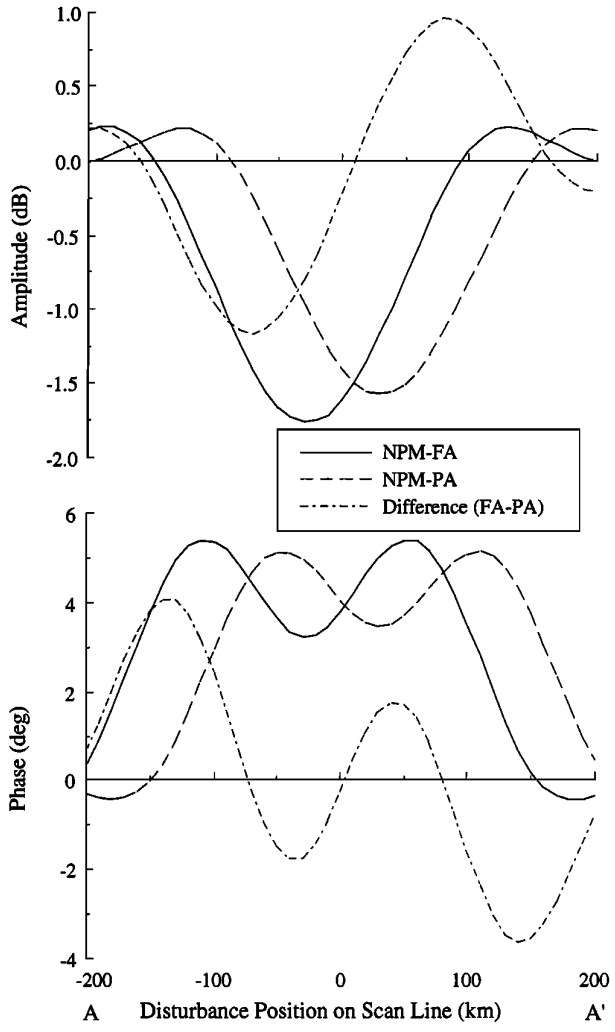

Figure 7. This figure is akin to Figure 6, but it shows the predicted changes on the (top) amplitude and (bottom) phase on both NPM-PA and NPM-FA when a 150-km-diameter disturbance and profile combination 3A are in effect. Also, the difference between the two curves in each plot ($\Delta A_{dif} \equiv \Delta A_{FA} - \Delta A_{PA}$ and $\Delta\Phi_{dif} \equiv \Delta\Phi_{FA} - \Delta\Phi_{PA}$) is shown.

exhibits a steady trend during the same period (Figure 2d). Considering Figure 7, the variation of the ΔA_{dif} values could be caused by a northward drift of LEP disturbance region and, therefore, an equatorward drift of the whistler-mode duct footprint, at a speed of ~100 km/hr. When this motion is mapped along the field lines into the equatorial plane it corresponds to a drift due to a westward electric field of about 0.4 mV/m which is of the expected order of magnitude at this local time under the prevailing moderately disturbed geomagnetic conditions (K_p = 3) [*Carpenter and Seely*, 1976; *Carpenter et al.*, 1979].

Although profile combination of 3A does provide the largest ΔA and $\Delta\Phi$ values for a given flux level and disturbance size, there is no independent means of determining the ambient profile in effect during this period. The ambient NPM signal levels observed at PA and FA during this period are not lower than usual, as would be expected in view of the null near the stations for this profile (Figure 5). It is thus possible that the ionospheric conditions were more similar to the ambient profile 1 or 2. In such a case the peak precipitation flux level of 5×10^{-3} ergs cm^{-2} s^{-1} would not produce results consistent with data. However, in view of the lack of knowledge of the flux level, a larger value such as 10^{-2} ergs cm^{-2} s^{-1} could well be in effect. Such a large flux level would yield a disturbance producing larger (doubled) signal changes [*Poulsen et al.*, 1993b] than those predicted previously with profiles 1 and 2 (for example see cases 1A and 2A with d = 300 km in Table 1). These values would be more consistent with the larger VLF signal amplitude and phase changes observed.

The sensitivity of the subionospheric VLF method of observation of ionospheric disturbances produced by LEP events, for extraction of information about the ambient ionospheric electron density profile and about the size and location of disturbances depends on several factors. The location of the disturbance transverse to the great circle paths can lead to signal amplitude and/or phase perturbations of positive or negative polarity; as seen from Figures 6–8, the different dependencies on the disturbance location of amplitude versus phase changes are consistent with the observed weak correlation between the magnitudes of simultaneous amplitude and phase events [*Wolf and Inan*, 1990]. The observation of a given ionospheric disturbance is greatly enhanced under those ambient ionospheric conditions that prevail when deep nulls in signal amplitude occur at or near the receiver (Figure 5). Conversely, for receiver locations near the crests of signal amplitude (such as that at 10.7 Mm from

Table 1. Amplitude and Phase Changes on NPM-PA

	d = 50 km		d = 150 km		d = 300 km	
Profile	ΔA, dB	$\Delta\Phi$, deg	ΔA, dB	$\Delta\Phi$, deg	ΔA, dB	$\Delta\Phi$, deg
1A	-0.07	-0.12	-0.59	0.15	-1.42	3.60
1B	-0.04	0.06	-0.32	1.15	-0.60	4.38
1C	-0.01	0.03	-0.09	0.43	-0.15	1.45
2A	-0.05	-0.13	-0.46	-0.25	-1.14	1.78
2B	-0.03	-0.00	-0.19	0.38	-0.42	1.86
2C	-0.01	0.00	-0.04	0.10	-0.07	0.39
3A	-0.19	0.00	-1.57	3.46	-3.25	20.47
3B	-0.05	0.14	-0.35	1.93	-0.57	6.44
3C	-0.01	0.02	-0.05	0.28	-0.08	0.88

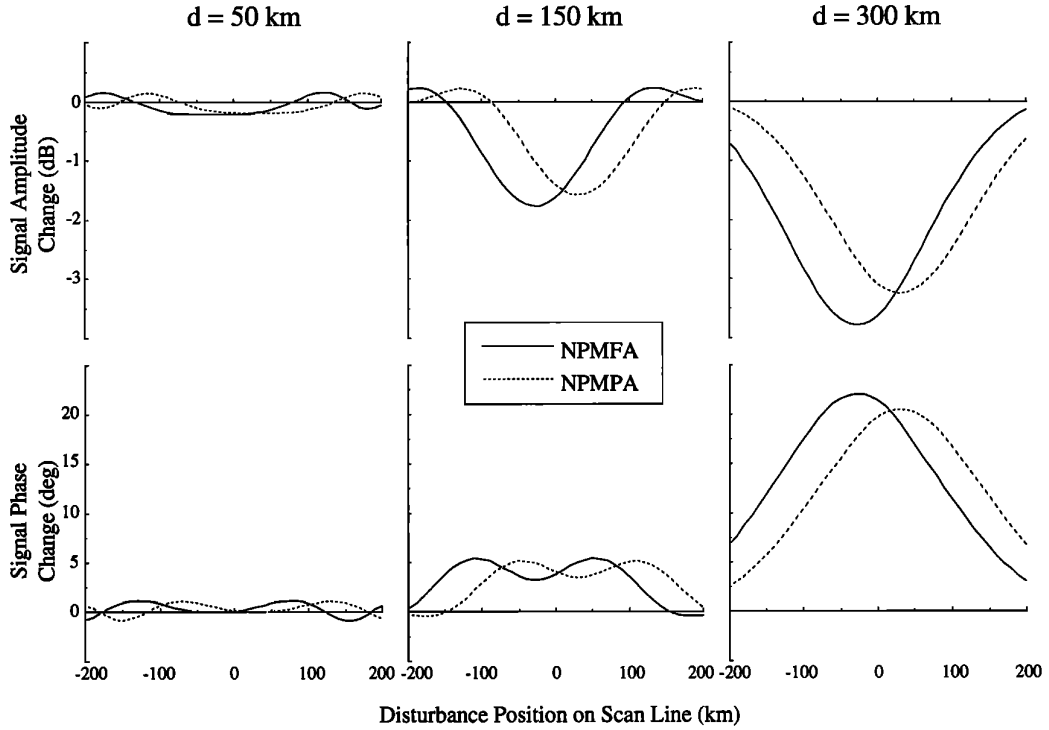

Figure 8. Comparison of LEP perturbations predicted for NPM-PA and NPM-FA when the disturbance diameter is 50, 150, and 300 km (by columns left to right). The top row shows the amplitude changes and the bottom row shows the phase changes expected as functions of disturbance location on the scan line AA′ (Figure 3).

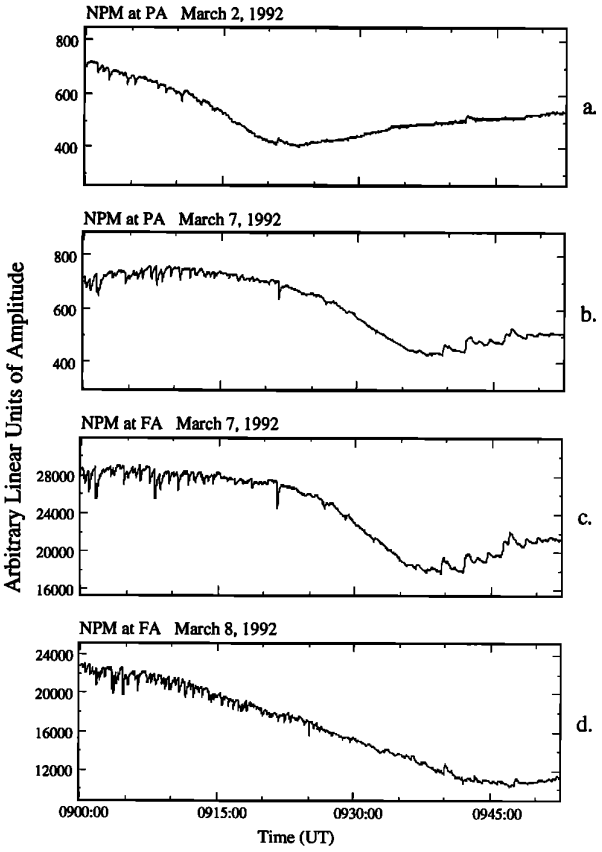

NPM in the lower left panel of Figure 5) we expect relatively small VLF perturbations for given ionospheric disturbances.

Since the whistler rate showed no signs of decreasing (from ~3.4 whistlers per minute) as daylight moved along the VLF paths and onto the disturbance location region (discussed further in next section), it is likely that LEP continued into the day. However, with VLF observations we are presently unable to detect the occurrence of LEP under daytime ionospheric conditions. This observation is important when considering the global effect of LEP on the loss rate of electrons from the Earth's radiation belts and the deposit of energy into the ionosphere from LEP: nighttime detection may need to be extrapolated to the daytime for accurate assessment of LEP's effect linking the ionosphere and the magnetosphere.

Effect of the Terminator

As pointed out previously, near the end of the episodes of LEP activity on the 3 days studied (from 0830 UT onward) the envelope of the negative amplitude perturbations tended to decrease in magnitude and then change sign to positive values (at ~0920 UT); meanwhile, the envelope of the phase perturbations, while remain-

Figure 9. Data showing the reversal of polarity of the LEP perturbations on the NPM signal amplitude at both receivers, and on different days. Note the fading of the signal amplitude characteristic of the day-night terminator moving onto the paths. All panels share the same time axis (although they are not all from the same day). (a) NPM-PA amplitude on March 2, 1992. (b) NPM-PA amplitude on March 7, 1992. (c) NPM-FA amplitude on March 7, 1992. (d) NPM-FA amplitude on March 8, 1992.

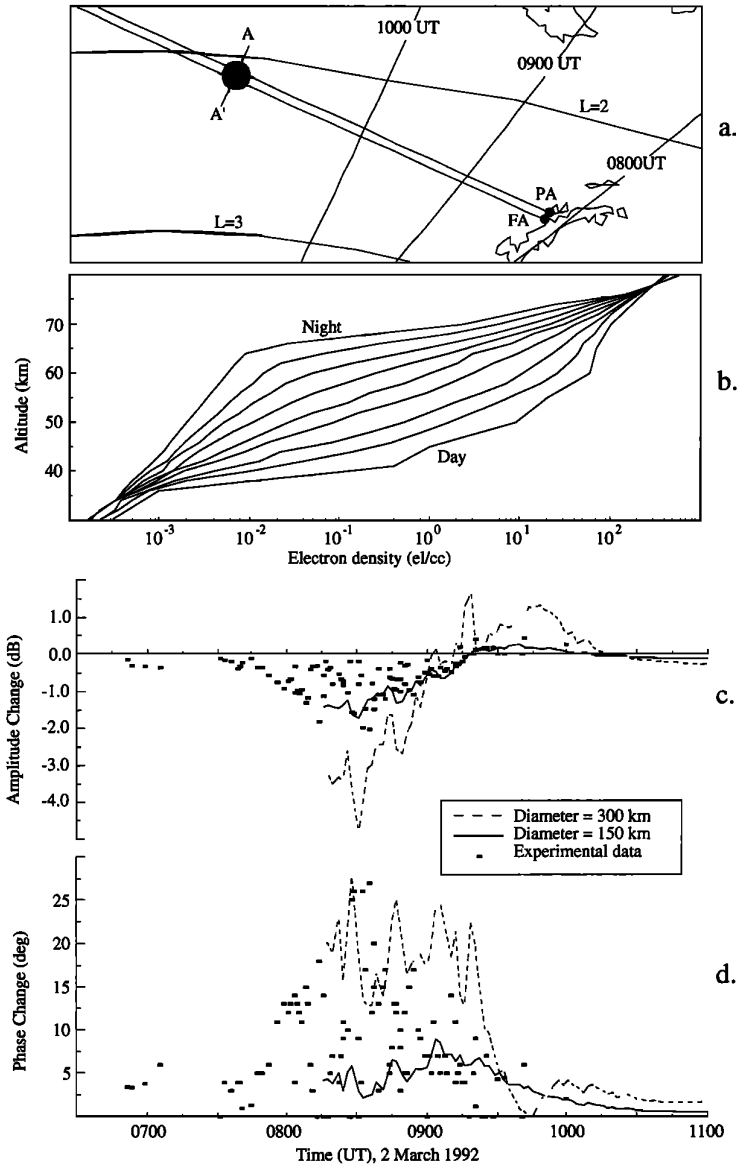

Figure 10. (a) Map showing the position of the terminator at three times during the episode of LEP activity on March 2, 1992. Other features shown are discussed in the caption for Figure 3. (b) Ionospheric electron density profiles showing the gradual transition from nighttime (profile 3 of Figure 4a) to daytime which were used to represent the day-night terminator in the modeling. The terminator was made up of seven 200-km-long segments (one for each intermediate profile shown) for a 1400-km-long transition region between night and day. (c) Predicted amplitude changes of the NPM signal at PA as a function of time (based on movement of the terminator) are shown as a continuous line for a disturbance 150 km in diameter, and as a broken line for a disturbance 300 km in diameter. This case uses ambient profile 3, disturbed profile A, and a disturbance located at the center of scan line AA′. Data from the episode of March 2, 1992 is shown for comparison as points. (d) The plot of phase changes which corresponds to Figure 10c.

ing positive, decreased in size on both paths (Figures 2a and 2b). The trend for the case of amplitude perturbations is illustrated in Figure 9. From Figure 10a, we see that the sunrise terminator at 100 km altitude was located between the disturbance and the receivers during the time that this transition from negative to positive amplitude perturbations occurred. This change in LEP signatures tended to occur during, and right after, the signal fading (at ~0920 UT in Figure 9) which is characteristic of the movement of the day-night terminator onto the paths [*Yokoyama and Tanimura*, 1933; *Crombie*, 1964, 1966].

We simulated the gradual transition from a nighttime to a daytime ionosphere along the NPM-PA path using seven 200-km segments to constitute the day-night transition over a distance of 1400 km. The ionospheric electron density profile was gradually changed from the nighttime ambient profile 3 to a daytime profile [*Reagan et al.*, 1981] (Figure 10b). Using the ambient ionosphere thus constructed, we computed the effect of disturbances having diameters of 150 and 300 km, and located at the center of the scan line AA′ (Figure 10a). Figures 10c and 10d show the amplitude and phase changes, respectively, as functions of time (each time corresponding to a different

position of the beginning of the 1400-km-long day/night transition) which are expected from the gradual movement of the day-night terminator along the NPM-PA path. For comparison, actual data points for March 2, 1992, are plotted from Figure 2. We see from Figure 10c that the overall trend of the envelope of the signal amplitude changes is consistent with that expected due to the motion of the day-night terminator, namely, the change from negative to positive values as the terminator moves along the NPM-PA path. While the range of ΔA values predicted for the 150-km-diameter disturbance (solid line) encompasses most of the data values, those for the 300-km disturbance lie generally above the range of values measured. Based on this, and for profile combination 3A and the flux value of 5×10^{-3} ergs cm^{-2} s^{-1} used, the disturbance size is likely to be between 200 and 300 km in diameter. In Figure 10d we see that the trend in the data toward smaller positive phase changes is supported by our model calculations. As indicated above with amplitude, the size of the disturbance is likely to have been 200–300 km in diameter. (It should be noted that the jaggedness of the lines in Figures 10c and 10d is due to the discrete jumps in ionospheric electron density profiles (Figure 10b): at each sudden jump in Earth-ionosphere waveguide characteristics, mode conversion yields scattering into higher order modes which combine to make rapidly changing values due to these modes' high attenuation rates with distance. With the actual terminator, the transition from night to day is smoother so that this jaggedness is but an artifact of our modeling.)

Summary

VLF signatures of LEP events have been simultaneously observed at two sites ~50 km apart and at $L \simeq 2.4$. The general behavior of the VLF amplitude and phase changes observed at the two sites was similar; however, measurable differences are apparent. Both the phase and amplitude changes themselves and the differences between the values observed at the two sites are found to be consistent with a relatively dense ambient nighttime D region electron density and a disturbance density profile that would be produced by precipitating electrons of >600 keV energy. Some of the amplitude and phase changes were quite large (−2.0 dB and +27°, respectively), which for reasonable assumptions about LEP burst flux levels correspond to ionospheric disturbances which had a transverse extent of 150–300 km and were located within ±200 km of the paths. Higher flux levels can account for the observations with more tenuous ambient nighttime D regions. The measured differences at the two observation sites can be explained by the transverse position of the LEP disturbance relative to the paths. The time variation of the differences between the amplitude changes at the two sites is consistent with motion of the whistler duct footprint northward across the paths at a speed of about 100 km/hr, corresponding to a magnetospheric westward electric field in the equatorial plane of about 0.4 mV/m. The observed overall trends in the envelopes of the changes are interpreted as being due to the movement of the day-night terminator onto the paths.

Acknowledgments. We thank Martin Walt for his comments on the manuscript and to our colleagues in the STAR Laboratory for useful discussions. This research was sponsored by the National Science Foundation under grant ATM-9113012.

The Editor thanks D. R. Moorcroft and L. J. Lanzerotti for their assistance in evaluating this paper.

References

Barr, R., M. T. Rietveld, P. Stubbe, and H. Kopka, The diffraction of VLF radio waves by a patch of ionosphere illuminated by a powerful HF transmitter, *J. Geophys. Res.*, *90*, 2861, 1985.

Burgess, W. C., and U. S. Inan, Simultaneous disturbance of conjugate ionospheric regions in association with individual lightning flashes, *Geophys. Res. Lett.*, *17*, 259, 1990.

Burgess, W. C., and U. S. Inan, The role of ducted whistlers in the precipitation loss and equilibrium flux of radiation belt electrons, *J. Geophys. Res.*, *98*, 15643, 1993.

Carpenter, D. L., Whistler studies of the plasmapause in the magnetosphere, 1, Temporal variations in the position of the knee and some evidence on plasma motions near the knee, *J. Geophys. Res.*, *71*, 693, 1966.

Carpenter, D. L., and J. W. LaBelle, A study of whistlers correlated with bursts of electron precipitation near $L = 2$, *J. Geophys. Res.*, *87*, 4427, 1982.

Carpenter, D. L., and N. T. Seely, Cross-L drifts in the outer plasmasphere: Quiet time patterns and some substorm effects, *J. Geophys. Res.*, *81*, 2728, 1976.

Carpenter, D. L., C. G. Park, and T. R. Miller, A model of substorm electric fields in the plasmasphere based on whistler data, *J. Geophys. Res.*, *84*, 6559, 1979.

Carpenter, D. L., U. S. Inan, E. W. Paschal, and A. J. Smith, A new VLF method for studying burst precipitation near the plasmapause, *J. Geophys. Res.*, *90*, 4128, 1985.

Chang, H. C., and U. S. Inan, Quasi-relativistic electron precipitation due to interactions with coherent VLF waves in the magnetosphere, *J. Geophys. Res.*, *88*, 318, 1983.

Chang, H. C., and U. S. Inan, Test particle modeling of wave-induced energetic electron precipitation, *J. Geophys. Res.*, *90*, 6409, 1985.

Crombie, D. D., Periodic fading of VLF signals received over long paths during sunrise and sunset, *J. Res. Natl. Bur. Stand. U.S., Sect. D*, *68D*, 27, 1964.

Crombie, D. D., Further observations of sunrise and sunset fading of very-low-frequency signals, *Radio Sci.*, *1*, 47, 1966.

Helliwell, R. A., J. P. Katsufrakis, and M. L. Trimpi, Whistler-induced amplitude perturbation in VLF propagation, *J. Geophys. Res.*, *78*, 4679, 1973.

Inan, U. S., and D. L. Carpenter, On the correlation of whistlers and associated subionospheric VLF/LF perturbations, *J. Geophys. Res.*, *91*, 3106, 1986.

Inan, U. S., and D. L. Carpenter, Lightning-induced electron precipitation events observed at $L \sim 2.4$ as phase and amplitude perturbations on subionospheric VLF signals, *J. Geophys. Res.*, *92*, 3293, 1987.

Inan, U. S., W. C. Burgess, T. G. Wolf, D. C. Shafer, and R. E. Orville, Lightning-associated precipitation of MeV electrons from the inner radiation belt, *Geophys. Res. Lett.*, *15*, 172, 1988a.

Inan, U. S., D. C. Shafer, and W.-Y. Yip, Subionospheric VLF signatures of nighttime D region perturbation in the vicinity of lightning discharges, *J. Geophys. Res.*, *93*, 11455, 1988b.

Inan, U. S., M. Walt, H. D. Voss, and W. L. Imhof, Energy spectra and pitch angle distributions of lightning-induced electron precipitation: Analysis of an event observed on the S81–1 (SEEP) satellite, *J. Geophys. Res.*, *94*, 1379, 1989.

Inan, U. S., F. A. Knifsend, and J. Oh, Subionospheric VLF "imaging" of lightning-induced electron precipitation from the magnetosphere, *J. Geophys. Res.*, *95*, 17217, 1990.

Inan, U. S., J. V. Rodriguez, S. Lev-Tov, and J. Oh, Ionospheric modification with a VLF transmitter, *Geophys. Res. Lett.*, *19*, 2071, 1992.

Lev-Tov, S. J., U. S. Inan, and T. F. Bell, Altitude profiles of localized D region density disturbances produced in lightning-induced electron precipitation events, *J. Geophys. Res.*, *100*, 21375, 1995.

Lohrey, B., and A. B. Kaiser, Whistler-induced anomalies in VLF propagation, *J. Geophys. Res.*, *84*, 5121, 1979.

Pasko, V. P., and U. S. Inan, Recovery signatures of lightning-associated VLF perturbations as a measure of the lower ionosphere, *J. Geophys. Res.*, *99*, 17523, 1994.

Poulsen, W. L., T. F. Bell, and U. S. Inan, Three-dimensional modeling of subionospheric VLF propagation in the presence of localized D region perturbations associated with lightning, *J. Geophys. Res.*, *95*, 2355, 1990.

Poulsen, W. L., T. F. Bell, and U. S. Inan, A multiple-mode three-dimensional model of VLF propagation in the earth-ionosphere waveguide in the presence of localized D region disturbances, *J. Geophys. Res.*, *98*, 1705, 1993a.

Poulsen, W. L., U. S. Inan, and T. F. Bell, The scattering of VLF waves by lo-

calized ionospheric disturbances produced by lightning-induced electron precipitation, *J. Geophys. Res.*, *98*, 15553, 1993b.

Rawer, K., D. Bilitza, and S. Ramakrishnan, Goals and status of the International Reference Ionosphere, *Rev. Geophys.*, *16*, 177, 1978.

Reagan, J. B., R. E. Meyerott, R. C. Gunton, W. L. Imhof, E. E. Gaines, and T. R. Larsen, Modeling of the ambient and disturbed ionospheric media pertinent to ELF/VLF propagation, paper presented at NATO-AGARD Meeting on Medium, Long, and Very Long Wave Propagation, Brussels, Belgium, Sept. 1981.

Rosenberg, T. J., R. A. Helliwell, and J. P. Katsufrakis, Electron precipitation associated with discrete very-low-frequency emissions, *J. Geophys. Res.*, *76*, 8445, 1971.

Tolstoy, A., The influence of localized precipitation-induced *D* region ionization enhancements on subionospheric VLF propagation, Ph.D. dissertation, Univ. of Maryland, College Park, 1983.

Tolstoy, A., J. J. Rosenberg, U. S. Inan, and D. L. Carpenter, Model predictions of subionospheric VLF signal perturbations resulting from localized, electron precipitation-induced ionization enhancement regions, *J. Geophys. Res.*, *91*, 13473, 1986.

Voss, H. D., W. L. Imhof, M. Walt, J. Mobilia, E. E. Gaines, U. S. Inan, R. A. Helliwell, and D. L. Carpenter, Energy and time structure of lightning-induced electron precipitation (abstract), *Eos Trans. AGU*, *66*, 350, 1985.

Wait, J. R., A possible mechanism for excessive mode conversion in the Earth-ionosphere waveguide, *Radio Sci.*, *1*, 1073, 1966.

Wait, J. R., and K. P. Spies, Influence of finite ground conductivity on the propagation of VLF radio waves, *Tech. Note 300*, Natl. Bur. of Stand., Washington, D. C., 1964.

Wait, J. R., and K. P. Spies, Characteristics of the Earth-ionosphere waveguide for VLF radio waves, *Radio Sci.*, *69D*, 1359, 1965.

Wolf, T. G., and U. S. Inan, Path-dependent properties of subionospheric VLF amplitude and phase perturbations associated with lightning, *J. Geophys. Res.*, *95*, 20997, 1990.

Yokoyama, E., and I. Tanimura, Some long-distance transmission phenomena of low-frequency waves, *Proc. IRE*, *21*, 263, 1933.

M. A. Clilverd and A. J. Smith, British Antarctic Survey, High Cross, Madingley Road, Cambridge CB3 0ET, England.

U. S. Inan and S. J. Lev-Tov, STAR Laboratory, Department of Electrical Engineering, Durand 324, Stanford University, Stanford, CA 94305-9515.

(Received November 27, 1995; revised February 21, 1996;
accepted March 25, 1996.)